Photochemical Charge Transfer and Hydrogen Evolution Mediated by Oxide Semiconductor Particles in Zeolite-Based Molecular Assemblies

Yeong Il Kim*

Department of Chemistry, National Fisheries Univeristy of Pusan, Daeyeon-dong, Nam-gu, Pusan 608-737, Korea

Steven W. Keller*

Department of Chemistry, University of Missouri−Columbia, Columbia, Missouri 65211

Jonathan S. Krueger and Edward H. Yonemoto

Department of Chemistry, University of Texas at Austin, Austin, Texas 78712

Geoffrey B. Saupe and Thomas E. Mallouk*

Department of Chemistry, The Pennsylvania State University, University Park, Pennsylvania 16802

Received: August 19, 1996; In Final Form: November 20, 1996[⊗]

Two integrated systems for light-induced vectorial electron transfer are described. Both utilize photosensitized semiconductor particles grown in linear channel zeolites as components of the electron transfer chain. One system consists of internally platinized zeolites L and mordenite containing TiO_2 particles and methylviologen ions, with a size-excluded photosensitizer, tris(2,2′-bipyridyl-4,4′-dicarboxylate)ruthenium (RuL_3^{2+}), adsorbed on the external surface of the zeolite/TiO_2 composite. In the other system, Nb_2O_5 replaces TiO_2. The kinetics of photochemical electron transfer reactions and charge separation were studied by diffuse reflectance flash photolysis. Despite very efficient initial charge separation, the TiO_2 system does not generate hydrogen photochemically in the presence of an electrochemically reversible, anionic electron donor, methoxyaniline *N*,*N*′-bis(ethyl sulfonate). Only the Nb_2O_5-containing composites evolved hydrogen photochemically under these conditions. These results are interpreted in terms of semiconductor band energetics and the irreversibility of electron transfer from Nb_2O_5 to intrazeolitic platinum particles.

Introduction

Progress on the challenging problem of solar energy conversion and storage has been made as a result of interdisciplinary efforts among several fields, including photochemistry, electrochemistry, solid state chemistry, and catalysis. There are essentially two viable approaches in photoconversion schemes: (1) generating electricity and (2) producing chemical fuels. Photoelectrochemical methods are now well established for both purposes,[1] having advanced to the point where liquid-junction cells are as efficient as or superior to Schottky-junction solid state cells.[2] Photosensitization of wide band gap semiconductor electrodes, as originally described by Gerischer,[3a] has been employed to make visible light usable as well as to avoid problems of photocorrosion that are often encountered with small band gap semiconductors. Extensive studies of organic dyes,[3] transition metal complexes,[4] phthalocyanines,[5] porphyrins,[6] and surface complexes[7] have been carried out to improve sensitization efficiencies for several types of semiconductors. Under short-circuit conditions, the photon-to-current conversion efficiency is very high for photosensitized TiO_2, approaching unity at low-light intensities (when corrected for reflection and absorption losses).[8]

The photosensitization of semiconductor colloids and particles is now well understood at a fundamental level.[9,10] By adding catalysts for hydrogen evolution to these particles, it is possible to create a particle-based system that is analogous to a dye-sensitized photoelectrochemical cell. Despite the successes achieved with photoelectrochemical cells, however, there have been very few reports of particle-based systems that use visible light to make energy-rich products photochemically, i.e., without the use of "sacrficial" reagents.[11] In a photoelectrochemical cell, oxidized and reduced products are formed at spatially well-separated electrodes, and so their recombination can be avoided easily. However, in photochemical systems, products are made at the same particle, or in the same homogeneous solution, and the recombination reaction, which is spontaneous in the thermodynamic sense, is much more difficult to prevent. Thus it is unreasonable to expect an efficient particle-based photochemical system without proper molecular-level design.

In this paper we describe a sensitized semiconductor-based electron transport chain that is spatially organized in a linear channel zeolite. Internally platinized zeolites L and mordenite, which have channel openings of 7.1 and 7.0 × 6.5 Å diameter, respectively, were loaded with oxide semiconductor (TiO_2 and Nb_2O_5) particles. A photosensitizer complex, tris(2,2′-bipyridyl-4,4′-dicarboxylate)ruthenium (RuL_3^{2+}), which is size-excluded from the zeolite pores, was adsorbed onto the semiconductor particles that are exposed at the zeolite external surface. Upon excitation of the sensitizer in the visible and subsequent electron transfer quenching by the semiconductor, electrons flow to internal catalytic sites where hydrogen is generated from water. An idealized drawing of this integrated photochemical system and its energetics are shown in Scheme 1. The system is designed to drive electrons photochemically from solution phase donors to intrazeolitic catalytic sites in a vectorial fashion and to result in hydrogen evolution without dark recombination of

[⊗] Abstract published in *Advance ACS Abstracts,* March 1, 1997.

S1089-5647(96)02539-4 CCC: $14.00 © 1997 American Chemical Society

SCHEME 1: Schematic Drawing and Relative Energetics of a Sensitized Semiconductor/Zeolite System for Photochemical Hydrogen Evolution

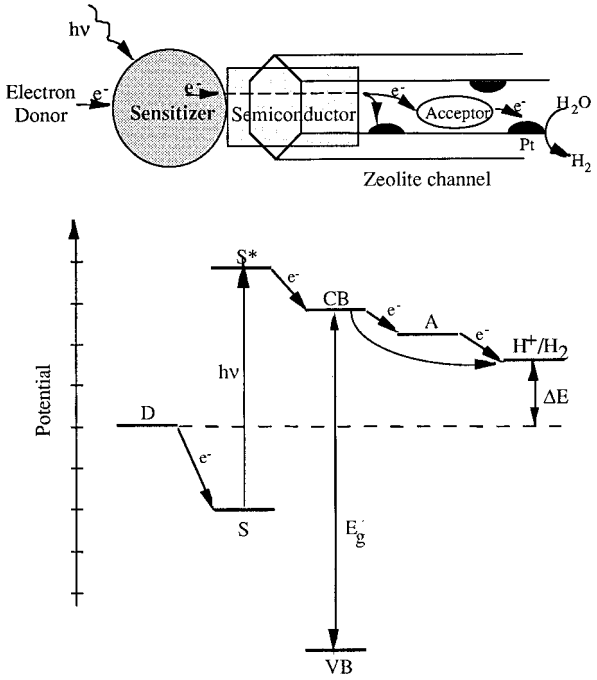

products. Attempts to generate hydrogen photochemically from electrochemically reversible electron donors in the TiO_2 system were unsuccessful. In the Nb_2O_5 system, however, small amounts of hydrogen are evolved from an electrochemically reversible donor. These results are rationalized in terms of semiconductor energetics, specifically in terms of the irreversibility of electron transfer from the semiconductor conduction band to the intrazeolitic platinum catalyst particles.

Experimental Section

Materials. Zeolite L (ideal formula $K_6Na_3Al_9Si_{27}O_{72}\cdot 21H_2O$) was purchased as a powder from Union Carbide, Linde Molecular Sieves division. The powdered synthetic mordenite, CBV 10A (ideal formula $Na_8Al_8Si_{40}O_{96}\cdot 24H_2O$), was a gift of the PQ Corporation. The average particle diameter of these zeolites, as determined by SEM, was roughly 1 μm. In order to remove ion-exchangeable impurities, predominantly extra-framework iron, all zeolite powders were stirred for several hours at 50 °C in 1 M aqueous NaCl solution. They were then washed copiously with H_2O until free of chloride ions, as determined via the silver nitrate test.

Methylviologen (MV^{2+}) dichloride hydrate was obtained from Aldrich and used as received. Propylviologen sulfonate was prepared according to the method of Maverick et al.[12] (Dicyanomethyl)viologen (DCV^{2+}) dibromide was prepared by refluxing 0.005 mol of 4,4′-bipyridine and 0.012 mol of bromoacetonitrile in 150 mL of CH_3CN for 2 days.

Tris(2,2′-bipyridyl-4,4′-dicarboxylate)ruthenium (RuL_3^{2+}) dichloride was prepared as follows: 1.2×10^{-3} mol of ruthenium(III) chloride and 3.6×10^{-3} mol of 4,4′-dicarboxy-2,2′-bipyridine were refluxed in 200 mL of 2-propanol/H_2O (10:1 v/v) with 0.5 g of Na_2CO_3 for 2 days. After filtration and removal of most of the solvent, the product was eluted from a silica gel column using CH_3CN/H_2O/saturated aqueous KNO_3 (5:4:1 v/v/v). The second red fraction, which luminesced, was collected; the first and remaining fractions were brown-colored and nonluminescent. Evaporating the solvent and adding acetone served to precipitate excess KNO_3 and Na_2CO_3. The

SCHEME 2: Procedure for Internal Platinization of Zeolite L and Mordenite

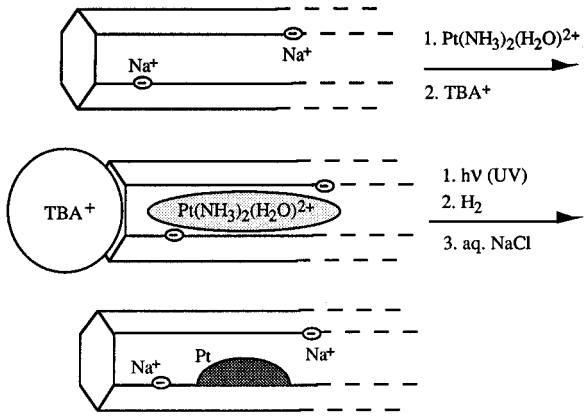

product was then precipitated from acetone by adding 6 M HCl until pH = 1−2. The filtered product was washed with acetone and dried at room temperature.

Titanium tetraisopropoxide, titanium tetrachloride, and niobium pentachloride were obtained from Aldrich; the $TiCl_4$ was vacuum-distilled twice before use. The preparation of *cis*-$[Pt(NH_3)_2I_2]$ was accomplished via the method of Dhara.[13]

Disodium methoxyaniline *N*,*N*′-bis(ethyl sulfonate) was prepared in the following manner: 20 g (0.189 mol) of sodium 2-bromoethanesulfonate, 11.67 g (0.095 mol) of *p*-anisidine, and 13.13 g of K_2CO_3 were dissolved in 400 mL of dry ethanol. The mixture was heated at reflux for 12 h and then cooled, and any solids remaining were filtered off. Following removal of the solvent, the product was recrystallized twice, first from boiling absolute ethanol and finally from ethanol/water (80:20 v/v).

All other chemicals were reagent grade and used as received from commercial sources. Water was deionized using a Barnstead Nanopure II system.

Platinization of Zeolites. A method for depositing elemental platinum at loadings of 0.01−0.1% by weight exclusively within the channels of mordenite and zeolite L is depicted in Scheme 2. The photochemically unstable precursor complex $Pt(NH_3)_2(H_2O)_2^{2+}$ is used. This procedure avoids high-temperature decomposition/reduction steps, which are known to cause sintering of small metal clusters and, invariably, migration of some of the clusters to the external surface of the zeolite.[23] A typical procedure for preparing 0.1 wt % of platinized zeolite was as follows: 25 mg (5.18×10^{-5} mol) of *cis*-$Pt(NH_3)_2I_2$ was suspended with 17 mg (1.0×10^{-4} mol) of $AgNO_3$ in 25 mL of H_2O at 52 ± 2 °C. In order to avoid excess Ag^+ in solution, a slightly substoichiometric amount of $AgNO_3$ was used. Vigorous stirring of this suspension gave a clear $Pt(NH_3)_2(H_2O)_2^{2+}(NO_3^-)_2$ solution and a greenish-yellow AgI precipitate. The filtered solution was added to a 150 mL aqueous suspension of 10 g of zeolite, stirred for 1 h, and allowed to stand for 1 day in the dark. To this suspension was added 0.4 g (1.24×10^{-3} mol) of tetrabutylammonium bromide (TBA^+Br^-) ; the purpose of this second ion exchange is to displace $Pt(NH_3)_2(H_2O)_2^{2+}$ ions on the external surface by size-excluded TBA^+. The suspension was stirred, left for 1 day in the dark, and the subsequently filtered solid was then washed several times with H_2O. The ion-exchanged zeolite containing $Pt(NH_3)_2(H_2O)_2^{2+}$ and TBA^+ was resuspended in 100 mL of H_2O and photolyzed in a quartz reaction vessel using an unfiltered 150 W Xe arc lamp for 10−15 h. After photolysis, the zeolite suspension was purged with H_2 at ambient temperature to give elemental platinum within the zeolite. In order to

TABLE 1: Summary of Preparative Conditions, Composition, and Sorption Properties of Mordenite/Oxide Semiconductor Composites

composite	precursor	loading (wt %)	sorption data (mol/g)		primary site of oxide particles
			MV^{2+}	RuL_3^{2+}	
T1	$Ti(OR)_4$	0.1−10	3.0×10^{-4}	$2-3 \times 10^{-6}$	external
T2	$TiCl_4$	3−7	1.5×10^{-4}	$2-3 \times 10^{-6}$	internal/external
N1	$Nb(OMe)_5py$	4−35	$<5 \times 10^{-7}$	8×10^{-7}	internal
N2	$NbCl_5$	4−35	4.3×10^{-5}	2×10^{-6}	internal/external

remove excess TBA^+ from the zeolite, the sample was resuspended in 100 mL of 1 M aqueous NaCl solution overnight, washed thoroughly, and dried at 40 °C in air. Samples prepared in this way were light gray in color and darker when higher loadings of Pt were used. The amount of $Pt(NH_3)_2(H_2O)_2^{2+}$ ion-exchanged into the zeolite was quantified spectrophotometrically using the $SnCl_2$ method.[14] The reported loading of elemental Pt in the zeolite was calculated from the amount of $Pt(NH_3)_2(H_2O)_2^{2+}$ taken up by the zeolite during the ion-exchange reaction.

Deposition of TiO_2 in/on Zeolites. Zeolite/TiO_2 composites were prepared from two different kinds of precursor, titanium tetraalkoxide (isopropoxide or ethoxide) and titanium tetrachloride. In the former case, a sol−gel method was used: 10 g of zeolite was dehydrated at 400 °C under vacuum and suspended in 150 mL of absolute ethanol or 2-propanol, and the desired amount of titanium tetraalkoxide was added. After the solution was stirred overnight, the solvent was removed by evacuation, and the sample was exposed to air. The hydrolysis of titanium tetraalkoxide in the air at room temperature gave zeolite/TiO_2 composite **T1**. The amount of TiO_2 was easily controlled by adding the appropriate amount of titanium tetraalkoxide.

In the second case, a gas phase impregnation method was used: 5 g of dehydrated zeolite was equilibrated for 8−10 h with dry N_2 or Ar which carried gaseous $TiCl_4$. The stream of gas passed through 10−15 mL of liquid $TiCl_4$ in a continuous flow (50−100 mL/min). Subsequent hydrolysis in an air stream at room temperature for 10−20 h gave zeolite/TiO_2 composite **T2**.[15] The amount of deposited TiO_2 could not be controlled precisely, but depended on the equilibration time and flow rate of the carrier gas. In this case TiO_2 was deposited in amounts of 3−7 wt %, typically. The composites were analyzed photocolorimetrically using hydrogen peroxide after the zeolite itself was dissolved in hot sulfuric acid.[16]

Deposition of Nb_2O_5 in/on Zeolites. The zeolite Nb_2O_5 composites were prepared from two different kinds of precursor, a niobium alkoxide and niobium pentachloride. In the former case, a sol−gel method was utilized: $NbCl_5$ (0.07 g, 2.56 mmol) was added to a Schlenk flask under argon and dissolved in 25 mL of dry MeOH. Pyridine (0.21 mL, 2.59 mmol) was added to this clear solution with stirring. Dissolution of $NbCl_5$ in MeOH forms the dimeric $Nb_2(OMe)_{10}$ complex, which is too large to be readily sorbed into the channels of mordenite. The addition of pyridine cleaves the dimer to produce $Nb(OMe)_5$·py.[17] The solution was transferred under Ar to another flask containing 1.50 g of dried mordenite. The slurry was stirred overnight under Ar and then evacuated to remove excess solvent. The resulting off-white mass was calcined at 400 °C in flowing air to form the zeolite/Nb_2O_5 composite **N1**.

In the second case, a vapor transport method was used: in an Ar-filled drybox, 2.00 g of dried mordenite and 0.70 g of $NbCl_5$ were charged to a thick-walled Pyrex tube fitted with a needle valve connection. The tube was connected to a stainless steel vacuum line and evacuated to <500 mTorr and then backfilled with Ar three times. Chlorine gas was then added to the evacuated sample to yield a final pressure of ∼400 Torr, and the tube was sealed. $NbCl_5$ sublimes as a dimer unless an atmosphere of Cl_2 is present.[18] The sealed tube was placed in a tube furnace at 260 °C for 24 h and then cooled. The tube was broken open, and moist air was allowed to flow over the pale yellow powder to hydrolyze the internally deposited $NbCl_5$, giving composite **N2**. Carrying out this hydrolysis at room temperature served to minimize migration to the external surface. Loadings for both methods were typically in the 4−35 wt % range.

The composition of samples **T1**, **T2**, **N1**, and **N2** is summarized in Table 1.

Loading of Sensitizer and MV^{2+} on/in Zeolite/Semiconductor Composites. RuL_3^{2+} was strongly adsorbed onto the zeolite/semiconductor composites at pH < 4.[4f] Appropriate volumes of a 1.2 mM stock solution of $RuL_3^{2+}(Cl^-)_2$ were added to a suspension of 1.0 g of zeolite/semiconductor composite in 20 mL of H_2O, and the suspension pH was adjusted to 4.0 using dilute $HClO_4$. After being stirred briefly, the bright red-colored zeolite/semiconductor/RuL_3^{2+} composite was filtered and washed with acidified, unbuffered H_2O (pH = 4). The amount of adsorbed dye depended on the amount of oxide semiconductor in the composite; this was determined spectrophotometrically from the washings using the extinction coefficient of RuL_3^{2+} at 466 nm (ϵ_{466nm} = 21 000 M^{-1} cm^{-1}).[19] Ion exchange of MV^{2+} into the composite and analysis for it was accomplished as follows. Appropriate volumes of a stock solution of MV^{2+} were added to a suspension containing 1.0 g of composite in 35 mL of H_2O. The suspension was stirred for several minutes at room temperature and then allowed to stand overnight. Samples were filtered, washed thoroughly with H_2O, and dried in air at 40 °C. The completeness of ion exchange was determined spectrophotometrically from the washings and the stock solutions (extinction coefficient for MV^{2+} ϵ_{257nm} = 20 700 M^{-1} cm^{-1}).

Apparatus. Steady state photolyses were carried out with a 150 W Xe, 200 W Hg, or 500 W Xe-Hg arc lamp (Ushio), equipped with a water filter. For band gap excitation of oxide semiconductors in the composites, a 360(±50) nm interference filter was used, while a 450(±50) nm interference filter or 420 nm cutoff filter was used for visible illumination. Light intensities were measured with a Coherent 210 power meter. For calculation of the quantum yield of evolved hydrogen, a ferrioxalate solution was used as an actinometer.[21] For photochemical hydrogen evolution, a 16 mL quartz reaction vessel with a flat window (2.3 cm^2), stoppered with a rubber septum, was used. The volume of the headspace in which gases were collected was 8 mL. The sample solution and headspace were thoroughly purged with Ar for 10−20 min before irradiation. The evolved H_2 was analyzed with a Varian 90-P gas chromatograph, using a 60/80 mesh 5A molecular sieve column, argon carrier gas, and a thermal conductivity detector interfaced to an HP 3390A integrator.

X-ray powder diffraction (XRD) patterns were obtained with a Philips diffractometer using monochromatized Cu Kα radiation. The experimental setup for diffuse reflectance laser flash photolysis has been described elsewhere.[20]

Results and Discussion

Characterization of Platinized Zeolites. The platinization method described in the Experimental Section gave exclusive deposition of Pt clusters within the channels of zeolite L and mordenite. By comparison, the thermal reduction of ion-exchanged $Pt(NH_3)_4^{2+}$ gave Pt on both internal and external sites in zeolites L and Y.[22] The selectivity for Pt at internal zeolite sites was checked by simple chemical tests: the catalytic reduction of methylviologen and ferricyanide by hydrogen (see eqs 1 and 2 below) were utilized as probes of Pt location in/on the zeolite particles.[22] When purged with hydrogen, an MV^{2+} solution containing platinized zeolite particles turns deep blue, due to catalytic reduction of the MV^{2+}molecules, which are small enough to easily enter the zeolite channels. However, the reduction of ferricyanide is extremely slow because these ions are excluded from the channels on the basis of their size and charge, and they therefore cannot access internally sited Pt clusters.

$$MV^{2+} + {}^1/_2H_2 \xrightarrow{Pt} MV^{\bullet+} + H^+ \quad (1)$$

$$Fe(CN)_6^{3-} + {}^1/_2H_2 \xrightarrow{Pt} Fe(CN)_6^{4-} + H^+ \quad (2)$$

UV−visible spectra of ferricyanide solution, before and after hydrogen purging of the solution in the presence of suspended platinized zeolites, verified that there was no reduction of ferricyanide and therefore no Pt at sites accessible to ferricyanide. The sensitivity of this test was calibrated using Pt supported on nonporous SiO_2 powder. Slow reduction of ferricyanide was observed for a loading of 6.0×10^{-6} wt %, but no reduction was observed at loadings 1 order of magnitude lower.[22] In the case of a 0.1 wt % of platinized zeolite sample, assuming similar degrees of Pt dispersion on the surfaces of SiO_2 and zeolite, we can therefore conclude that externally sited Pt on the zeolite comprises less than 0.006% of the total platinum. The platinum loading level in zeolite L and mordenite using this method can be varied easily up to the maximum ion-exchange capacity of the zeolites for $Pt(NH_3)_2(H_2O)_2^{2+}$ (which is ca. 3.0×10^{-4} mol/g). However, good selectivity for Pt deposition at internal sites, as determined by the ferricyanide test, was limited to a maximum loading of about 0.1 wt % of Pt. At this loading, the reproducibility of sample preparation was low, while samples with less than 0.05 wt % of Pt were highly reproducible and always gave a negative test for externally sited platinum. Although the exclusivity of internal siting is lost at higher platinum loading, our platinization method seems to give more well-dispersed platinum clusters inside the zeolite channels than those in the thermal reduction method using the $Pt(NH_3)_4^{2+}$precursor. Thermal treatment at high temperatures causes platinum to migrate and coalesce into larger clusters.[23]

Characterization of Zeolite/Semiconductor Composites. It is difficult to characterize the location, size, and crystallinity of TiO_2 and Nb_2O_5 in the zeolite/semiconductor composites. X-ray diffraction patterns are essentially identical to those of the zeolite only, and there are no additional peaks assignable to TiO_2 or Nb_2O_5, for composites **T1**, **T2**, **N1**, and **N2**. Therefore, TiO_2 and Nb_2O_5 do not order within the cages of the composites, and oxide semiconductor particles deposited on the external surface either are amorphous or consist of crystallites too small to be detected. In composite **T1**, because titanium tetraalkoxides exist as oligomers in alcohol solvents and because these oligomers are larger than the zeolite pore openings, we would expect most of the TiO_2 to be deposited on the external surface. In composite **T2**, which is prepared from $TiCl_4$, we would expect TiO_2 to be deposited primarily inside the channels because of the small size of the precursor.

The degree of pore filling of the composites was assessed by ion exchange of MV^{2+}, and the data are summarized in Table 1. The composite **T1** was loaded easily to a level of 3.0×10^{-4} mol of MV^{2+} per gram of composite, regardless of the presence of Pt and TiO_2 at 0.1 and 10 wt %, respectively. This is very near the maximum MV^{2+} capacity for mordenite itself, 3.4×10^{-4} mol/g.[20] In constrast, the composite **T2** had a maximum MV^{2+} loading level of ca. 1.5×10^{-4} mol/g in the case of a 5 wt % of TiO_2 sample. This implies that TiO_2 either occupies a significant fraction of the channel volume or blocks access of MV^{2+} to the channels in composite **T2**. A 35 wt % of Nb_2O_5 sample of composite **N1** exchanged no detectable amounts of MV^{2+}. In comparison, a 35 wt % of Nb_2O_5 sample of composite **N2** typically exchanged 4.3×10^{-5} mol of MV^{2+} per gram of composite. The drastically curtailed exchange capacity of **N1** is taken as evidence that Nb_2O_5 occupies essentially all zeolite internal volume. The decreased ion-exchange capacity of composite **T2** with MV^{2+} implies partial pore blocking, or filling of a substantial fraction of the pore volume, by TiO_2. These conclusions must be drawn cautiously since aluminum leaching from the zeolite framework can also occur in the presence of Lewis acids such as $SiCl_4$, and it is possible that exposure to $TiCl_4$ (or its hydrolysis product, HCl) causes a decrease in ion-exchange capacity. Because mordenite is by far the more acid-stable of the two zeolites used, it was used in all photolysis experiments.

Adsorption of RuL_3^{2+}, which is size-excluded from the zeolites, also gives an indication of the sites predominantly occupied by the semiconductor particles. In the case of a 10 and 7 wt % of TiO_2 composites **T1** and **T2**, typically $2-3 \times 10^{-6}$ mol of RuL_3^{2+} were adsorbed per gram. This value corresponds to monolayer coverage of the zeolite external surface and implies that the surface area of exposed TiO_2 is roughly equivalent to that of the parent zeolite. For the Nb_2O_5 composites, the amount of sensitizer adsorbed depended upon the method of preparation. For example, in the case of a 35 wt % of Nb_2O_5 composite **N1**, typically 8×10^{-7} mol of RuL_3^{2+} was adsorbed per gram of composite, whereas in the case of a 35 wt % of Nb_2O_5 composite **N2**, the value was 2×10^{-6} mol/g of RuL_3^{2+}. This difference is consistent with more complete encapsulation of the semiconductor particles in the case of **N1**. In the absence of TiO_2 or Nb_2O_5, RuL_3^{2+} does not adsorb onto the zeolite even at pH 2. However, if the suspension is allowed to stand overnight at this pH, the complex is partially co-precipitated with zeolite.

Figure 1 shows diffuse reflectance UV−visible absorption spectra of mordenite/TiO_2 composite **T1** and bulk TiO_2 (anatase). The absorption spectrum of zeolite/TiO_2 composite **T2** is not significantly different from that of **T1**. Also, there are no noticeable differences between spectra obtained with zeolite L and mordenite. The spectra are plotted as the Kubelka−Munk function $F(R)$, which is proportional to the concentration of absorbing species. When compared with bulk anatase, the absorption edge of mordenite/TiO_2 is blue-shifted by about 30 nm. The band gap energy of TiO_2 in the composite can be estimated, based on the following relation between absorption coefficient α and band gap energy E_g:

$$\alpha \propto (h\nu - E_g)^{n/2} \quad (3)$$

where $n = 1$ for direct band gap materials and $n = 4$ for indirect band gap materials.[24] Since TiO_2 is considered to be an indirect band gap material,[25] plots of the square root of $F(R)$ vs photon

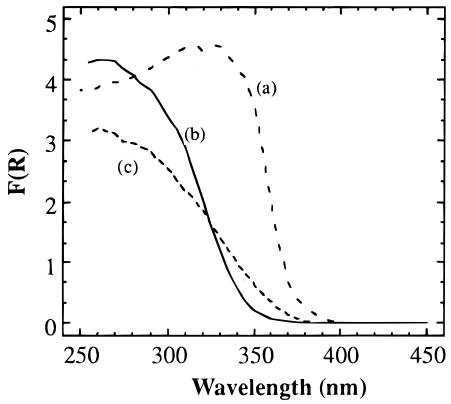

Figure 1. Diffuse reflectance UV−visible spectra of (a) bulk TiO_2 (anatase), (b) mordenite/TiO_2 prepared from a solution of Ti(OCH-$(CH_3)CH_3)_4$, and (c) after annealing the sample in (b) at 400 °C for 6 h.

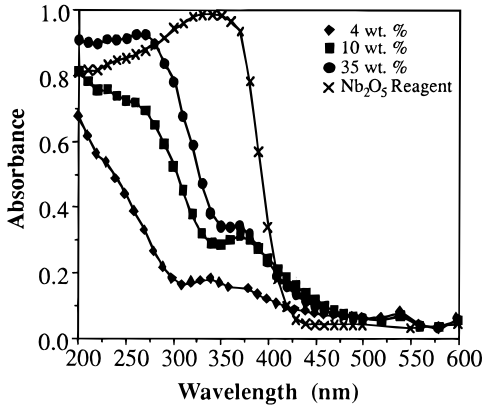

Figure 2. Diffuse reflectance UV−visible spectra of 4, 10, and 35 wt % of Nb_2O_5 composites **N2** (from mordenite) compared to that of bulk Nb_2O_5.

energy were used to calculate band gap energies of approximately 3.5 eV in the mordenite/TiO_2 composites and 3.3 eV for anatase TiO_2. The latter is in agreement with the literature value for anatase TiO_2. It should be noted that these values derive largely from the long-wavelength tail of the semiconductor absorbance and therefore reflect primarily the largest particles in the distribution. Thus, there may be a distribution of particle sizes produced by these techniques, with small particles (i.e., those inside the cages) absorbing only to the blue of the observed absorption edge.

TiO_2 incorporated into the interlayer spaces of montmorillonite has been shown to have a larger band gap than that of anatase, and the increased band gap was interpreted in terms of a quantum size effect.[26] The increased band gap energy of TiO_2 in the zeolite composite is also likely due to size quantization, either from confinement of the semiconductor to the channels or from small particle size on the external surface.

For comparison purposes, bulk TiO_2 was prepared from a titanium isopropoxide sol in absolute ethanol, without the zeolite host, by air hydrolysis at room temperature. This TiO_2 gave almost the same absorption onset as the zeolite/TiO_2 composites, indicating that it also had a larger band gap, and no peaks were observable in its XRD pattern. When this bulk TiO_2 sample was annealed above 400 °C in air, the absorption onset shifted to the red and XRD peaks corresponding to the anatase form appeared as broad lines. These diffraction peaks sharpened as temperature and annealing time were increased. While this bulk TiO_2 appeared amorphous before annealing, it may possess anatase microcrystalline domains since there was no sharp transition between the amorphous and anatase diffraction patterns.

When the zeolite/TiO_2 composite **T1** was annealed at 400 °C for several hours, the absorption edge was also red-shifted close to that of anatase, as shown in spectrum c of Figure 1. As far as its crystallinity is concerned, the TiO_2 in zeolite composite **T1** might be considered to have the same quality as that of bulk TiO_2 prepared from a titania sol; in other words, the increased band gap can be attributed to size-quantized microcrystallites, but not simply to confinement of TiO_2 to the zeolite channels. However, the TiO_2 in composite **T1** appears to be well dispersed on the external surface of the zeolite and does not block the pore openings significantly.

Figure 2 compares the diffuse reflectance spectra of composites **N2** having 4, 10, and 35 wt % of Nb_2O_5 to that of bulk Nb_2O_5. All three composite samples are blue-shifted with respect to the bulk; lower loadings of semiconductor result in a shift to progressively shorter wavelengths of absorption onset. Such shifts are again taken to be indications that the Nb_2O_5 particles are in the so-called quantum size regime and on average become larger at higher loadings. The shoulder at 360 nm may also indicate the presence of somewhat larger particles, perhaps agglomerates on the surface.

If we assume that the increased band gap in the composites is due to size quantization, whether they are confined to the zeolite channels or not, the size of semiconductor microcrystallites can be estimated from the "particle-in-a-sphere" formula given by Brus:[27c]

$$\Delta E_g = \frac{\pi^2 h^2}{2R^2}\left[\frac{1}{m_e^*} + \frac{1}{m_h^*}\right] - \frac{1.8e^2}{\epsilon_R} + \text{polarization terms} \quad (4)$$

where R is a radius of the semiconductor particle and m_e^* and m_h^* are effective masses of the electron and hole in the semiconductor. Because the optical dielectric constant of bulk TiO_2 is very large ($\epsilon = 170$), the Coulombic and polarization terms in the equation are neglected. Using $m_e^* = 20m_e$ and $m_h^* = 3m_e$ and taking $\Delta E_g = 0.2$ eV, the largest TiO_2 microcrystallites in the composites have a diameter of ca. 17 Å.[28]

Wang et al. have modified the particle-in-a-sphere model for the size dependence of semiconductor band gaps by including the effect of band nonparabolicity.[29] The observed band gaps for PbS nanoparticles incorporated in polymer films was well explained by this model, while eq 4 gave significant errors. In this hyperbolic band model, the band gap of a semiconductor particle of radius R is given by the following:

$$E_g' = [E_g^2 + (2h^2/m^*)(\pi/R)^2 E_g]^{1/2} \quad (5)$$

Here $1/m^*$ is the average of the reciprocals of the electron and hole masses and E_g is the band gap of the bulk semiconductor. Assuming $m^* \approx m_h^* = 3m_e$, the largest particles of TiO_2 in the zeolite composites are estimated from eq 5 to be ca. 20 Å. Note that both models give maximum particle size values which are significantly in excess of the size of the 12 rings that interconnect cages in zeolite L and mordenite. We might conclude from this that some larger particles have formed on the external surface of the zeolite and/or that there is strong electronic interaction between semiconductor particles within the zeolite. If the particles within are interconnected, much in the same way as the zeolite channels are interconnected, then their effective (electronic) size could be significantly larger than the channel window dimensions.

If the increased band gap of the zeolite/TiO_2 composite is due to a quantum size effect, then it should be possible to

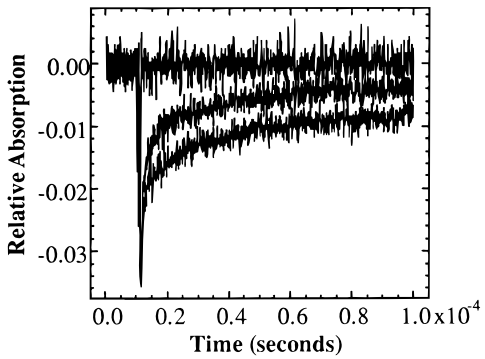

Figure 3. Transient diffuse reflectance signals of mordenite/TiO_2 (**T1**)/RuL_3^{2+} in (from bottom) H_2O, 1.0 M TEOA, and 0.1 M KI solutions (pH = 3.8), monitored at 466 nm. Excitation source: 11 ns laser pulse at 532 nm.

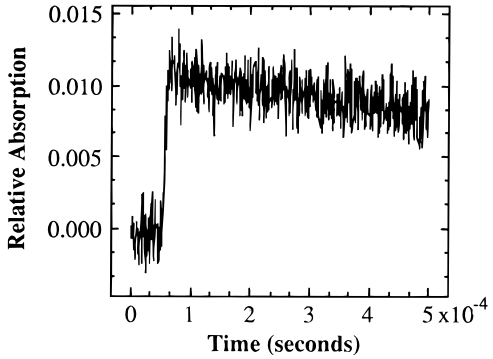

Figure 4. Diffuse reflectance transient absorption signal of mordenite/TiO_2 (**T1**)/RuL_3^{2+} in 0.1 M KI solution (pH = 3.8), monitored at 380 nm (the absorption maximum of $I_2^{-\bullet}$). Excitation source: 11 ns laser pulse at 532 nm.

evaluate the conduction band edge shift according to the theory of size quantization.[26] The ratio of the shift of conduction band edge potential to the shift of valence band edge caused by size quantization, $\Delta E_c/\Delta E_v$, is given by $(\Delta E_g)(m_h^*/m_e^*)$, where ΔE_g is the increase in band gap energy and m_e^* and m_h^* are effective masses of the electron and hole in the semiconductor, respectively. Assuming $m_e^* = 20m_e$ and $m_h^* = 3m_e$ and taking $\Delta E_g = 0.2$ eV, the conduction band edge of the zeolite/TiO_2 composite is expected to be only 16 mV more negative than that of bulk anatase TiO_2. For single-crystal rutile TiO_2, E_{fb} has been found to be in the range 0.06 to −0.05 V vs NHE at pH = 0.[30] Similarly, the conduction band edge potential of the zeolite/Nb_2O_5 composites is expected to be only slightly negative of that of bulk Nb_2O_5.

Diffuse Reflectance Flash Photolysis of Sensitized Zeolite/Oxide Semiconductor Composites. When the size-excluded photosensitizer RuL_3^{2+} was adsorbed onto the surface of the TiO_2 and Nb_2O_5 composites, the luminescence of the Ru complex was quenched by charge injection into the conduction band of the oxide semiconductor. Sensitization of this type has been previously studied with colloidal TiO_2.[8,9,31] Diffuse reflectance flash photolysis was used to observe bleaching of the ground state of the complex by monitoring absorbance changes at 466 nm after a laser pulse at 532 nm (see Figure 3). Some of the bleaching recovery occurs on a short time scale (less than 0.5 μs) and may be an artifact of scattering of the laser flash and emission of excited state RuL_3^{2+}. The remaining slow decay is due to charge recombination of the injected electron and the oxidized complex. Although the kinetics of this recombination (subtracted from the initial fast component) do not follow single-exponential kinetics, its time scale is clearly in the submillisecond range. This long-lived charge separation was observed for both **T1** and **T2**, with very similar decay kinetics for both zeolite hosts.

In the case of colloidal TiO_2, Kalyanasundaram et al.[32] have reported that recombination occurs with a rate constant of 4×10^5 s^{-1}. The recombination in the sensitized zeolite/TiO_2 composite appears to be about 100 times slower than that with colloidal TiO_2. Considering the sensitizer's emission rate ($\sim 10^7 s^{-1}$) as the lower limit for the charge injection rate from the excited Ru complex to TiO_2, the charge recombination rate is at least 4 orders of magnitude slower than the forward electron transfer rate. The nonlinearity of the recovery could be due to inhomogeneity of adsorption sites on the TiO_2 surface or to a multiplicity of pathways for the charge recombination reaction.

The effects of electron donors on the bleaching recovery are also evident in Figure 3. While the long time component of the signal completely disappears in a solution of 0.1 M iodide, which is a chemically reversible electron donor, the recovery rate was shortened only by about half in the presence of 1.0 M triethanolamine (TEOA), a sacrificial electron donor. The shortening of the bleaching recovery in electron donor solutions is attributed to reduction of the oxidized Ru complex. These results indicate that reduction by TEOA is much slower than by iodide, implying that TEOA will be a less effective electron donor than is iodide in steady state photolysis. It was found that sacrificial electron donors such as TEOA, EDTA, cysteine, and dithiothreitol were generally less effective (at pH < 4) for reduction of the oxidized Ru complex than were reversible electron donors such as iodide, potassium 2,5-dihydroxy-1,4-benzenedisulfonate, potassium 2,5-dihydroquinonesulfonate, and potassium *N*,*N*,*N*′,*N*′-tetraethylsulfonate−phenylenediamine. Kinetic studies of $Ru(bpy)_3^{3+}$ reduction by TEOA and EDTA have shown that electron transfer rates decrease by an order of magnitude as the pH decreases by 2 units.[32] Deprotonation of these basic sacrificial electron donors makes them good reducing agents, and they are ineffective in cases where low pH conditions are needed to ensure adsorption of the sensitizer and quenching of its excited state by oxide semiconductor particles.

When iodide was the donor, formation of $I_2^{-\bullet}$ was observed spectroscopically at 380 nm, simultaneous with the reduction of the oxidized Ru complex (see Figure 4). Over the time scale available with our instrument (which was limited to 0.5 ms by lamp pulse stability), it is difficult to discern the kinetics of $I_2^{-\bullet}$ decay. Considering the recombination between the injected electron and $I_2^{-\bullet}$ juxtaposed with the likely disproportionation reaction of $I_2^{-\bullet}$ to I_3^-, the kinetics should be complex.[33] Apart from these kinetic details, we conclude that the charge-separated state, consisting of $I_2^{-\bullet}$ and the conduction band electron in the zeolite/TiO_2 composite, persists for as long as several milliseconds.

When a cationic electron acceptor of suitable size and proper redox potential is ion-exchanged into the channels of the zeolite/semiconductor composite, electron transfer from the conduction band to the acceptor is possible. This electron transfer reaction was studied using methylviologen and (dicyanomethyl)viologen (DCV^{2+}) [redox potentials −0.44 and −0.17 V vs NHE, respectively] as electron acceptors. In diffuse reflectance flash photolysis experiments, a reduced viologen signal was observed in an aqueous suspension of a DCV^{2+}-loaded zeolite L/TiO_2/RuL_3^{2+} composite **T1** (pH = 4) following laser excitation at 532 nm. Figure 5 shows (a) the transient absorption spectrum and (b) the signal of reduced (dicyanomethyl)viologen at 400 nm for such a composite.

Because the RuL_3^{2+} adsorbs only on the TiO_2 surface of the composite and does not desorb from the composite at pH 4, the observed reduced viologen can be attributed to electron transfer mediated by the conduction band of TiO_2. We assume

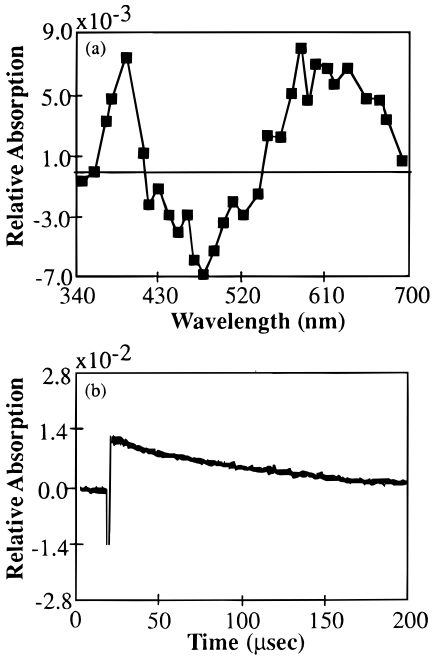

Figure 5. Diffuse reflectance transient spectrum (a) and absorption signal at 400 nm (b) in an aqueous suspension of a zeolite L/TiO_2/RuL_3^{2+}/DCV^{2+} composite (pH = 4). The spectrum was recorded 67 μs after a 532 nm laser pulse and corrected for the wavelength dependence of the path length of the analyzing light as described previously.[11b]

that there is little direct quenching of the sensitizer excited state by DCV^{2+} in the composite since luminescence quenching by TiO_2 is rapid. The decay of reduced DCV^{2+} follows apparently single-exponential kinetics, with a lifetime of 120 μs. Since there may be traces of oxygen in the zeolite channels under these conditions, the actual lifetime may be even longer than this.

When this composite was ion-exchanged with MV^{2+}, which has a potential 0.28 V higher than that for DCV^{2+}, we observed no photoreduced $MV^{+\bullet}$ (regardless of which zeolite was used in the composite). The results indicate that the electrons transiently injected into TiO_2 from the Ru complex have a potential sufficiently negative to reduce DCV^{2+}, but not MV^{2+}, at this pH. This could be due to two effects. First, the conduction band edge of TiO_2 in the composite may not be negative enough to reduce MV^{2+} at pH 4. Second, there are mid gap states on the surface of the TiO_2, the potential of these states is between the reduction potentials of MV^{2+} and DCV^{2+}, and the injected electrons are trapped there.

Photochemical Hydrogen Evolution. When *internally platinized* zeolite/semiconductor composites were irradiated by UV light in an aqueous sacrificial electron donor solution, molecular hydrogen was generated. Figure 6 shows plots of hydrogen evolution vs time for the internally platinized composite **T2** with/without ion-exchanged MV^{2+} and composite **T1** under irradiation of UV light. We may draw several conclusions from these data. First, there is significant contact between internal platinum and TiO_2 in both composites **T1** and **T2**, which were prepared from $Ti(OCH(CH_3)_2)_4$ and $TiCl_4$, respectively, because unplatinized zeolite/TiO_2 composites gave only traces of hydrogen under similar conditions. Second, despite the higher loading of TiO_2 in composite **T1**, the hydrogen evolution rate is higher that that in composite **T2**. This indicates that the TiO_2 in composite **T2** has better contact with internally sited platinum, consistent with the smaller size of the $TiCl_4$ precursor and lower capacity for MV^{2+} exchange observed for composite **T2**. Third, there is a significant contribution of MV^{2+} to the hydrogen

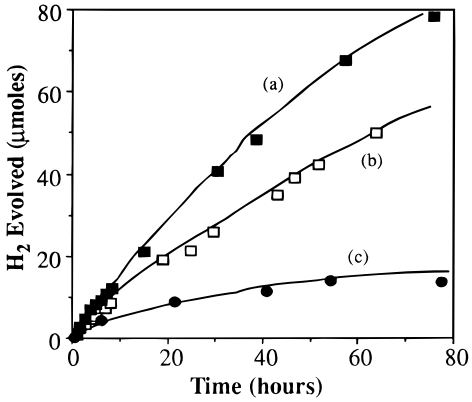

Figure 6. Plots of H_2 evolved vs time from 0.1 g of mordenite/Pt/TiO_2 composites in 8 mL of 2.0 mM EDTA solution (pH = 4.0) during irradiation (with interference filter 364 ± 50 nm, measured intensity 125 mW): (a) mordenite/TiO_2 (**T2**, 4.4 wt %)/Pt (0.1 wt %)/MV^{2+} (1.22×10^{-4} mol/g); (b) the same as (a) but without MV^{2+}; (c) mordenite/TiO_2 (**T1**, 6.7 wt %)/Pt (0.1 wt %).

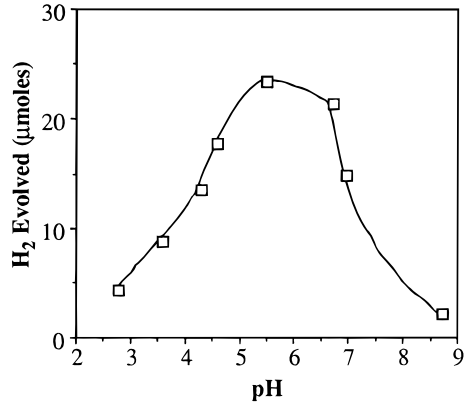

Figure 7. pH dependence of the hydrogen evolution rate from mordenite/TiO_2 (**T1**, 10 wt %)/Pt (0.1 wt %)/MV^{2+} (3.0×10^{-4} mol/g) in 10 mM TEOA solution. The pH was adjusted with HCl and NaOH.

evolution rate with composite **T2**. In this case, MV^{2+} seems to play a role as electron mediator between TiO_2 and the internal platinum clusters.

With MV^{2+} as a mediator for electron transport between TiO_2 and Pt in the composite, the hydrogen evolution rate will depend strongly on the pH of the solution. Because both the electron quasi-Fermi level of the TiO_2 and the proton reduction potential change by −0.059 V per pH unit, but the reduction potential of MV^{2+} does not, an optimum pH must be found where the MV^{2+} potential is intermediate between E_f* of TiO_2 and the proton reduction potential. The pH dependence of hydrogen evolution in the mordenite/TiO_2 (**T1**)/Pt/MV^{2+} composite is plotted in Figure 7. The highest hydrogen evolution rate is found at about pH 6.

Figure 8 gives plots of hydrogen evolution vs time for composites **N1** and **N2** under UV irradiation in the presence of methanol, which acts as a sacrificial electron donor. **N2** is significantly more active than **N1**. As noted in the Experimental Section, **N1** and **N2** differ in how the semiconductor is distributed on the zeolite particle—**N1** has Nb_2O_5 located almost exclusively within the zeolite channels, as reflected in its inability to exchange MV^{2+} and the low capacity for adsorbing RuL_3^{2+}. **N2** has more Nb_2O_5 located on the outside of the zeolite particle, as reflected in its greater capacity for RuL_3^{2+} adsorption. Furthermore, **N2** is able to exchange small amounts of MV^{2+}, and this implies that MeOH should also be able to penetrate any available void spaces in **N2**, thereby accessing a relatively large surface area of Nb_2O_5. **N1** is relatively

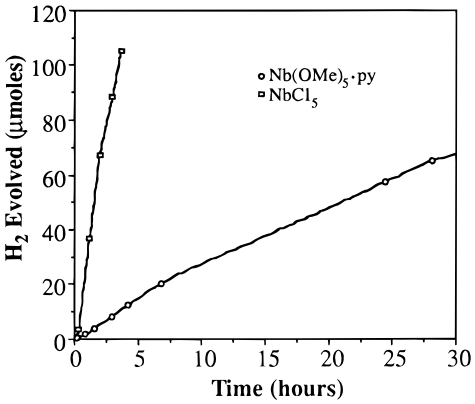

Figure 8. Plots of H_2 evolved vs time from 0.1 g of mordenite/Nb_2O_5 (35 wt %)/Pt (0.02 wt %) composites in 8 mL of aqueous MeOH solution (pH = 3.0) during UV irradiation: circles indicate **N1**; squares indicate **N2**.

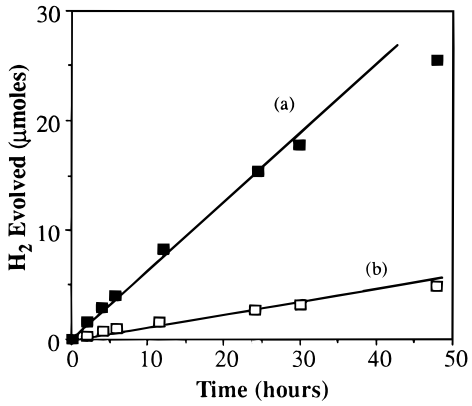

Figure 9. Plots of H_2 evolved vs time for 0.1 g samples of mordenite/TiO_2 (**T1**, 10.6 wt %)/Pt (0.1 wt %)/RuL_3^{2+} (2.5×10^{-6} mol/g) in 10 mM TEOA solution (pH = 4.0) during visible illumination ($\lambda \geq 400$ nm, effective light intensity < 20 mW): (a) with MV^{2+} (3.0×10^{-6} mol/g) and (b) without MV^{2+}.

impervious, and access of MeOH to the intrazeolitic Nb_2O_5 particles may be more restricted.

When the size-excluded photosensitizer RuL_3^{2+} was adsorbed onto the surface of zeolite/TiO_2 composites, visible illumination (>400 nm) also gave hydrogen evolution from sacrificial donors such as EDTA, TEOA, and dithiothreitol. Figure 9 shows a plot of hydrogen evolved vs time from 0.1 g of composite **T1**, with and without MV^{2+}, in 10 mM TEOA solution. Control experiments establish that no hydrogen is evolved if any of the essential components (RuL_3^{2+}, TiO_2, or Pt) are eliminated from the composite, and indeed RuL_3^{2+} does not adhere to the zeolite in the absence of TiO_2.

As demonstrated by the diffuse reflectance flash photolysis experiments, hydrogen evolution may be attributed to electron transfer quenching of photoexcited RuL_3^{2+} by TiO_2. Again, the presence of MV^{2+} in the channels significantly enhances the reaction rate, apparently by mediating electron transfer from TiO_2 to Pt. This would appear to contradict the flash photolysis experiments in which no $MV^{+\bullet}$ transient was observed. If the conduction band edge potential of TiO_2 in the composite is close to the reduction potential of MV^{2+} at this acidic pH, electron transfer between them could be slow. In this situation the detection of $MV^{+\bullet}$ by transient spectroscopy, especially in diffuse reflectance mode where the signal/noise ratio is low, might be very difficult. However, in steady state photolysis, conduction band electrons can accumulate in the presence of sacrificial donors and then have sufficient driving force to reduce MV^{2+}.

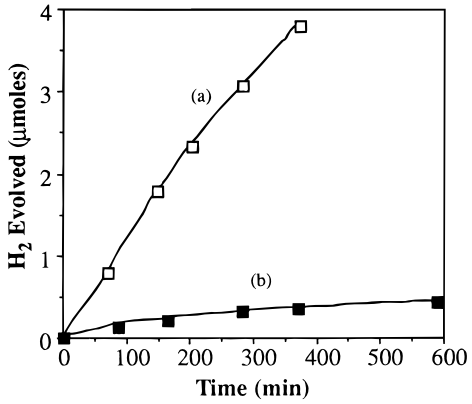

Figure 10. Plots of H_2 evolved vs time from (a) sensitized mordenite/TiO_2/Pt composite **T2** and (b) sensitized mordenite/TiO_2/Pt composite **T1** in 10 mM dithiothreitol (pH = 3.8) under visible illumination ($\lambda \geq$ 420 nm). The loadings of Pt, TiO_2, and RuL_3^{2+} are 0.1 wt %, 3.9 wt %, and 4.0×10^{-7} mol/g, respectively, in both cases.

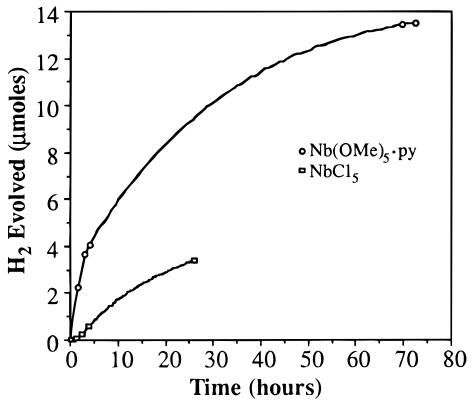

Figure 11. Plots of H_2 evolved vs time from sensitized, platinized composites **N1** and **N2** in 10 mM EDTA (pH = 3.0) under visible illumination ($\lambda = 450 \pm 50$ nm). The loadings of Pt, Nb_2O_5, and RuL_3^{2+} are 0.02 wt %, 35 wt %, and 5×10^{-7} mol/g, respectively, in both cases.

Figure 10 shows hydrogen evolution from composites **T1** and **T2** which were prepared from $Ti(OCH_2(CH_3)_2)_4$ and $TiCl_4$, respectively. Here, composite **T2** shows a much higher hydrogen evolution rate than that for composite **T1**, confirming that **T2** has more TiO_2 inside the zeolite channels and more efficient contact between the sensitized semiconductor and internal Pt.

Figure 11 shows the time course of photochemical hydrogen evolution for sensitized, platinized composites **N1** and **N2** during irradiation with visible light in the presence of the sacrificial electron donor EDTA. Interestingly, **N1** is more efficient than **N2** for visible light photolysis. This is the opposite of the case for UV photolysis, where **N2** was the more efficient photocatalyst. This might be explained on the basis of more efficient contact between Nb_2O_5 and Pt in composite **N1**. During visible photolysis, the RuL_3^{2+} sensitizer is the initial photon absorber, *not* the Nb_2O_5. Therefore, the amount of semiconductor surface area available for contact with the sacrificial donor is no longer critical in determining the kinetics of hydrogen evolution. Although significantly less RuL_3^{2+} is able to adsorb to the surface of **N1**, compared with **N2**, this factor is apparently not as important in determining maximal hydrogen evolution rate as is efficient transmission of conduction band electrons to Pt catalytic sites. Here, **N1** is likely to have the advantage, due to the dense packing of Nb_2O_5 in intrazeolite void spaces which the $Nb(OMe)_5$·py precursor apparently enables.

To elucidate the importance of initial charge separation between RuL_3^{2+} and TiO_2 in hydrogen evolution, photolyses

were carried out with internally platinized zeolite L and mordenite in which $Ru(bpy)_3^{2+}$ and MV^{2+} were self-assembled onto/into the zeolites, as described by Kim et al.[20] Na_2EDTA and appropriate amounts of acid were added to the solutions in order to provide a source of electrons. Only traces of hydrogen were found after 2 days of visible illumination. Most of the $Ru(bpy)_3^{2+}$ ions were desorbed from the surface of the zeolite during the photolysis. This desorption of $Ru(bpy)_3^{2+}$ from the surface of the zeolite (which is not observed in zeolite/TiO_2 composites sensitized by RuL_3^{2+}) was caused by the presence of Na^+, which is the counterion of $EDTA^{2-}$. The quenching of photoexcited solution-phase $Ru(bpy)_3^{2+}$ by MV^{2+} in the zeolite is very inefficient, although the cage escape yield of $Ru(bpy)_3^{3+}$ and $MV^{+\bullet}$ in zeolite L is known to be ca. 7%.[20] So the $Ru(bpy)_3^{2+}/MV^{2+}$ model system for artificial photosynthesis, while interesting in terms of photoinduced charge separation, is ineffective for hydrogen evolution under these conditions.

The quantum yield for hydrogen evolution by the zeolite/TiO_2/Pt/MV^{2+}/ RuL_3^{2+} composites in the presence of sacrificial donors was approximately 1% at 450 ± 5 nm, under partially optimized conditions. The low quantum yield of this system can be attributed to slow kinetics for reduction of the oxidized Ru complex by sacrificial donors (TEOA and EDTA), as confirmed by the flash photolysis experiments, and it can also be attributed to the low loading and activity of catalytic platinum sites. Mid gap states of TiO_2 in the composite, which can trap electrons photoinjected by RuL_3^{2+}, might also contribute to the low quantum yield.

Despite spatial separation of the hydrogen evolution catalyst and electron donors, very efficient reduction of the oxidized sensitizer by reversible electron donors, and slow charge recombination, hydrogen evolution from **T1** and **T2** was not observed at all in the presence of reversible electron donors such as iodide, 2,5-dihydroxy-1,4-benzenedisulfonic acid, hydroquinonesulfonic acid, sodium 4-methoxybenzeneamine *N*,*N*-bis(ethyl sulfonate), and potassium phenylenediamine-*N*,*N*,*N*′,*N*′-tetrakis(ethyl sulfonate). This has several possible causes: First, the mid gap states of TiO_2 reside at a potential that is not negative enough to reduce water, but is negative enough to reduce the oxidized donor. These states could then trap the injected electrons, and slow recombination between trapped electrons and the oxidized donor could occur. Second, the recombination of oxidized donor and hydrogen could be catalyzed by TiO_2 (we exclude donor/conduction band electron geminate recombination as a possible cause since the oxidized donor was spectroscopically observed on very long time scales). Although the catalytic sites for hydrogen evolution are physically inaccessible to the donor anions, TiO_2 is exposed to the solution at the external surface of the zeolite. If the conduction band edge potential of TiO_2 is close to the hydrogen/water formal potential, TiO_2 could mediate reverse electron transfer between the platinum catalyst and the solution-phase donor molecules.

The latter mechanism was indeed confirmed by the ferricyanide test (eq 2), performed on an internally platinized sample of zeolite L/TiO_2 composite **T1** when catalytic hydrogen reduction of ferricyanide occurred (see Figure 12). However, ferricyanide was not reduced in a suspension of the unplatinized composite **T1** (apparent absorptions below 350 nm were due to light scattering and absorption by the small zeolite/TiO_2 particles). Similar results were obtained with platinized **T2**/mordenite samples. Interestingly, platinized **N2**/mordenite does not catalyze the reduction of ferricyanide by hydrogen. While the high temperature used in the preparation of composite **N2** could cause some sintering or migration of Pt clusters, it is unlikely that this is the source of the dark recombination reaction with **T1** and **T2**, since the latter samples were prepared at ambient temperature.

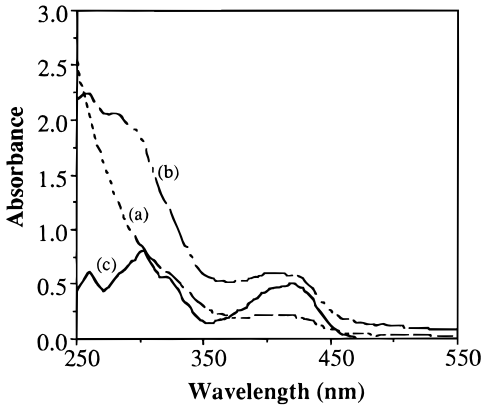

Figure 12. UV spectra of (a) 0.7 mM $Fe(CN)_6^{3-}$, (b) the same solution after purging with H_2 for 1 h in the presence of 50 mg of zeolite L/TiO_2 (**T1**, 10 wt %) composite, and (c) after purging with H_2 for 1 h in the presence of 50 mg of zeolite L/TiO_2 (**T1**, 10 wt %)/Pt (0.02 wt %) composite.

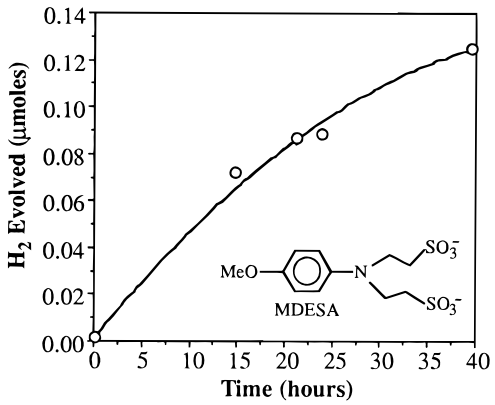

Figure 13. Plot of H_2 evolution vs time for 0.08 g of mordenite/Nb_2O_5/Pt/RuL_3^{2+} composite **N2** in 10 mM $MDESA^{2-}$ (pH = 3.0) during visible illumination (450 ± 50 nm).

While photolysis of water using oxide semiconductors and sacrificial electron donors is of basic interest, a practical solar energy conversion scheme will demand nonsacrificial electron donors that can be recycled chemically or electrochemically. The positive ferricyanide test in the case of platinized composite **T1** shows that the conduction band of TiO_2 is approximately coincident with the hydrogen/water potential. Figure 13 provides evidence that the conduction band edge potential of Nb_2O_5 is sufficiently negative that the dark recombination of H_2 and oxidized donor cannot be mediated by the semiconductor. A sample of mordenite/Nb_2O_5/Pt composite **N2**, sensitized with RuL_3^{2+} and irradiated with visible light in the presence of the nonsacrificial electron donor disodium methoxyaniline *N*,*N*-bis(ethyl sulfonate) ($MDESA^{2-}$), produced small amounts of hydrogen. It should be noted that the quantum efficiency for hydrogen production in this case is only about 0.01%. The quantum efficiency for hydrogen evolution from the same composite using the sacrificial donor EDTA, and under otherwise identical photolysis conditions, is approximately 1%. In other words, we observe a 2 order of magnitude decrease in quantum efficiency in using a nonsacrificial donor with the Nb_2O_5 system.

The reasons for this reduced efficiency, as compared with that of the sacrificial donor case, are currently under study. Again, mid gap states of the semiconductor could be involved in trapping injected electrons; these trapped electrons could

subsequently recombine with the oxidized donor on a relatively slow time scale. It is also conceivable that geminate recombination between $MDESA^{-\bullet}$ and conduction band electrons is significantly eroding quantum efficiency for the Nb_2O_5 system. This latter mechanism was ruled out for the TiO_2 systems because oxidized donor was observed spectroscopically on very long time scales.

Conclusions

In this paper we have described an *integrated chemical system*[34] for hydrogen evolution which utilizes photosensitized oxide semiconductors. The system is spatially organized by a linear channel zeolite (zeolite L or mordenite) into a vectorial array of electron donor/sensitizer/semiconductor/electron acceptor/catalyst. The ion-exchange properties and size-exclusion effects of the zeolite cause the donor, sensitizer, and acceptor to occupy their appropriate places in the electron transport chain. Photosensitization of TiO_2 or Nb_2O_5 by RuL_3^{2+} makes initial charge separation reasonably efficient (the lifetime of charge separation was in the submillisecond range) and makes the composite responsive to light of visible wavelengths. However, TiO_2 was found to mediate electron transfer in both directions, precluding the use of nonsacrificial electron donors with a TiO_2-containing system. As the root of this problem is the coincidence of the TiO_2 conduction band edge potential with the hydrogen potential, intrazeolite semiconductors with more negative conduction band edge potentials represent a potential solution. It was found that Nb_2O_5-containing systems evolve hydrogen in the presence of a non-sacrificial electron donor during visible illumination, albeit at a very low rate. The preparation of composites with appropriate combinations of donor, sensitizer, semiconductor, and catalyst-containing microporous substrates remains a significant challenge.

Acknowledgment. This work was supported by the Division of Chemical Sciences, Office of Basic Energy Sciences, Department of Energy, under contract DE-FG02-93ER14374. J.S.K. thanks Professor John T. McDevitt for many helpful conversations. Also, the technical assistance of Mr. Jeff Eubanks at Varian Corp. is gratefully acknowledged. This paper is dedicated to the memory of Heinz Gerischer.

References and Notes

(1) (a) Nozik, A. J. *Annu. Rev. Phys. Chem.* **1978**, *29*, 189. (b) Wrighton, M. S. *Acc. Chem. Res.* **1979**, *12*, 303. (c) Bard, A. J. *Science* **1980**, *207*, 139. (d) Heller, A. *Acc. Chem. Res.* **1981**, *14*, 154. (e) *Energy Resources Through Photochemistry and Catalysis*; Grätzel, M., Ed.; Academic Press: New York, 1983. (f) *Photochemical Energy Conversion*; Norris, J. R., Meisel, D., Eds.; Elsevier Science: New York, 1989.

(2) (a) Tufts, B. J.; Abrahams, I. J.; Santangelo, P. G.; Ryba, G. N.; Casagrande, L. G.; Lewis, N. S. *Nature* **1987**, *326*, 861. (b) Abrahams, I. L.; Santangelo, P. G.; Tufts, B. J.; Lewis, N. S. *New J. Chem.* **1987**, *11*, 157.

(3) (a) Gerischer, H. *Photochem. Photobiol.* **1972**, *16*, 243. (b) Gerischer, H.; Willing, F. *Topics Curr. Chem.* **1976**, *61*, 31. (c) Arden, W.; Fromherz, P. *J. Electrochem. Soc.* **1980**, *127*, 370. (d) Arden, W.; Fromherz, P. *Ber. Bunsen-Ges. Phys. Chem.* **1978**, *82*, 868. (e) Osa, T.; Fujihira, M. *Nature* **1976**, *264*, 349. (f) Memming, R. *Photochem. Photobiol.* **1972**, *16*, 325.

(4) (a) Gleria, M.; Memming, R. Z. *Phys. Chem. Neue Folge* **1975**, *98*, 302. (b) Clark, W. D. K. *J. Am. Chem. Soc.* **1977**, *99*, 4676. (c) Memming, R.; Schröppel, F.; Bringmann, U. *J. Electroanal. Chem.* **1979**, *100*, 307. (d) Hamnett, A.; Dare-Edwards, M. P.; Wright, R. D.; Seddon, K. R.; Goodenough, J. B. *J. Phys. Chem.* **1979**, *83*, 3280. (e) Dare-Edwards, M. P.; Goodenough, J. B.; Hamnett, A.; Seddon, K. R.; Wright, R. D. *Faraday Discuss. Chem. Soc.* **1980,** *70*, 285.

(5) (a) Jaeger, C. D.; Fan, F.-R. F.; Bard, A. J. *J. Am. Chem. Soc.* **1980**, *102*, 2592. (b) Giraudeau, A.; Fan, F.-R. F.; Bard, A. J. *J. Am. Chem. Soc.* **1980**, *102*, 5137. (c) Darwent, J. R.; Douglas, P; Harriman, A.; Porter, G.; Richoux, M. C. *Coord. Chem. Rev.* **1982**, *44*, 83.

(6) (a) Breddels, P. A.; Blase, G. *Chem. Phys. Lett.* **1981**, *79*, 209. (b) Kalyanasundram, K.; Vlachopoulos, N.; Krishnan, V.; Monnier, A.; Grätzel, M. *J. Phys. Chem.* **1987**, *91*, 2342.

(7) (a) Vrachnou, E.; Grätzel, M.; McEvoy, A. J. *J. Electranal. Chem.* **1989**, *258*, 193. (b) Vrachnou, E.; Vlachopoulos, N.; Grätzel, M. *J. Chem. Soc., Chem. Commun.* **1987**, 868. (c) Frei, H.; Fitzmaurice, D. J.; Grätzel, M. *Langmuir* **1990**, *6*, 198.

(8) (a) Duonghong, D.; Serpone, N.; Grätzel, M. *Helv. Chim. Acta* **1984**, *67*, 1012. (b) Desilvestro, J.; Grätzel, M.; Kavan, L.; Moser, J. *J. Am. Chem. Soc.* **1985**, *107*, 2988. (c) Furlong, D. N.; Wells, D.; Sasse, W. H. F. *J. Phys. Chem.* **1986**, *90*, 1107. (d) Vlachapoulos, N.; Liska, P.; Augustynski, J.; Grätzel, M. *J. Am. Chem. Soc.* **1988**, *110*, 1216. (e) Liska, P.; Vlachopoulos, N.; Nazeeruddin, M. K.; Comte, P.; Grätzel, M. *J. Am. Chem. Soc.* **1988**, *110*, 3686. (f) Amadelli, R.; Argazzi, R.; Bignozzi, C. A.; Scandola, F. *J. Am. Chem. Soc.* **1990**, *112*, 7099. (g) O'Regan, B.; Grätzel, M. *Nature* **1991**, *353*, 737. (h) Nazeeruddin, M. K.; Kay, A.; Rodicio, I.; Humphry-Baker, R.; Müller, E.; Liska, P.; Vlachopoulos, N.; Grätzel, M. *J. Am. Chem. Soc.* **1993**, *115*, 6382. (i) Pechy, P.; Rotzinger, F. P.; Nazeeruddin, M. K.; Kohle, O.; Zakeeruddin, S. M.; Humphry-Baker, R.; Grätzel, M. *J. Chem. Soc., Chem. Commun.* **1995**, 65. (j) Hagfeldt, A.; Grätzel, M. *Chem. Rev.* **1995**, *95*, 49.

(9) (a) Kamat, P. V. *Chem. Rev.* **1993**, *93*, 267. (b) Kamat, P. V.; In *Kinetics and Catalysis in Microheterogeneous Media*; Grätzel, M., Kalyanasundaram, K., Eds.; Marcel Dekker: New York, 1991; pp 376−436.

(10) (a) Kalyanasundaram, K. *Photochemistry in Microheterogeneous Systems*; Academic Press: Orlando, 1987. (b) Grätzel, M. *Heterogeneous Photochemical Electron Transfer*; CRC: Boca Raton, FL, 1989.

(11) (a) Kim, Y. I.; Salim, S.; Huq, M. J.; Mallouk, T. E. *J. Am. Chem. Soc.* **1991**, *113*, 9561. (b) Kim, Y. I.; Atherton, S. J.; Brigham, E. S.; Mallouk, T. E. *J. Phys. Chem.* **1993**, *97*, 11802.

(12) Maverick, A. W.; Najdzionek, J. S.; Mackenzie, D.; Nocera, D. G.; Gray, H. B. *J. Am. Chem. Soc.* **1983**, *105*, 1878.

(13) Dhara, S. C. *Indian J. Chem.* **1970**, *8*, 193.

(14) Ginzburg, S. I.; Ezerskaya, N. A.; Prokof'eva, I. V.; Fedorenko, N. A.; Shtenskaya, V. I.; Bel'skii, N. K. *Analytical Chemistry of Platinum Metals*; John Wiley & Sons, Inc.: New York, 1975.

(15) Komarov, V. S.; Shirinskaya, L. P.; Bokhan, N. P. *Russ. J. Phys. Chem.* **1976**, *50*, 1478.

(16) Marczenko, Z. *Spectrophotometric Determination of Elements*; John Wiley & Sons, Inc.: New York, 1976.

(17) Cotton, F. A.; Wilkinson, G. *Advanced Inorganic Chemistry*, 5th ed.; Wiley Interscience: New York, 1988; p 793.

(18) Greenwood, N. N.; Earnshaw, A. *Chemistry of the Elements*; Pergamon Press: Oxford, 1984; p 1153.

(19) Vlachopoulos, N.; Liska, P.; Augustynski, J.; Grätzel, M. *J. Am. Chem. Soc.* **1988**, *110*, 1216.

(20) Kim, Y. I.; Mallouk, T. E. *J. Phys. Chem.* **1992**, *96*, 2879.

(21) Gordon, A. J.; Ford, R. A. *The Chemist's Companion*; John Wiley & Sons, Inc.: New York, 1972.

(22) Persaud, L.; Bard, A. J.; Campion, A.; Fox, M. A.; Mallouk, T. E.; Webber, S. E.; White, J. M. *Inorg. Chem.* **1987**, *26*, 3825.

(23) Pan, M; Cowley, J. M.; Chan, I. Y. *Catal. Lett.* **1990**, *5*, 1.

(24) Butler, M. A. *J. Appl. Phys.* **1977**, *48*, 1914.

(25) Koffyberg, F. P.; Dwight, K.; Wold, A. *Solid State Commun.* **1979**, *30*, 433.

(26) Yoneyama, H.; Haga, S.; Yamanaka, S. *J. Phys. Chem.* **1989**, *93*, 4833.

(27) (a) Brus, L. E. *J. Chem. Phys.* **1984**, *80*, 4403. (b) Rossetti, R; Hull, R; Gibson, J. M.; Brus, L. E. *J. Chem. Phys.* **1985**, *83*, 1406. (c) Brus, L. E. *J. Phys. Chem.* **1986**, *90*, 2555.

(28) (a) Itakura, M; Niizuka, N.; Toyoda, H; Iwasaki, H. *Jpn. J. Appl. Phys.* **1967**, *6*, 311. (b) Kasinski, J. J.; Gomez-Juan, L. A.; Faran, K. J.; Gracewski, S. M.; Miller, R. J. D. *J. Chem. Phys.* **1989**, *90*, 1253.

(29) Wang, Y; Suna, A; Mahler, W; Kasowski, R. *J. Chem. Phys.* **1987**, *87*, 7315.

(30) Morrison, S. R. *Electrochemistry at Semiconductor and Oxidized Metal Electrodes*; Plenum: New York, 1980.

(31) Fitzmaurice, D. J.; Frei, H. *Langmuir* **1991**, *7*, 1129.

(32) (a) Kalyanasundaram, K; Kiwi, J; Grätzel, M. *Helv. Chim. Acta* **1978**, *61*, 2720. (b) Miller, D.; McLendon, G. *Inorg. Chem.* **1981**, *20*, 950.

(33) Grossweiner, L. I.; Matheson, M. S. *J. Phys. Chem.* **1957**, *61*, 1089.

(34) Bard, A. J. *Integrated Chemical Systems: A Chemical Approach to Nanotechnology*, John Wiley & Sons, Inc.: New York , **1994**.